



3D micro-printed polymer limacon-shaped whispering-gallery-mode microlaser sensors for label-free biodetection

ZHIZHENG WANG,^{1,†} MOHSIN RAZA,^{1,†} BIN ZHOU,¹ NAN WANG,^{1,2}
KUMMARA VENKATA KRISHNAIAH,^{1,2} YUWEN QIN,¹ AND A. PING ZHANG^{1,*}

¹ Photonics Research Institute, Department of Electrical and Electronic Engineering, The Hong Kong Polytechnic University, Kowloon, Hong Kong SAR, China

² Guangdong Provincial Key Laboratory of Information Photonics Technology, School of Information Engineering, Guangdong University of Technology, Guangzhou, China

[†] These authors contributed equally to this work.

*azhang@polyu.edu.hk

Received 20 January 2025; revised 18 March 2025; accepted 25 March 2025; posted 27 March 2025; published 16 May 2025

Optical whispering-gallery-mode (WGM) microlaser sensors have garnered significant attention in biological sensing due to their distinct advantages, including strong light–matter interactions and versatile sensing modalities. However, challenges remain in developing WGM microlaser sensors that can serve as building blocks for large-scale integrated sensor platforms in lab-on-chip applications. In this work, we present a 3D micro-printed polymer limacon-shaped WGM microlaser sensor for on-chip integrated biosensing. The WGM microlaser sensor has both high-quality factor (Q factor) and directional emission properties, making it ideal for high-sensitive on-chip biosensing platforms using a far-field coupling scheme. Experimental results showed that the 3D micro-printed WGM laser sensor has a very low lasing threshold of $3.87 \mu\text{J/mm}^2$ and a narrow lasing linewidth of about 30 pm. Remarkably, experiments have shown that the sensor can detect human IgG with a detection limit of around 70 ag/mL, revealing its potential for ultralow-limit detection of biomarkers in early disease diagnosis. © 2025 Optica Publishing Group. All rights, including for text and data mining (TDM), Artificial Intelligence (AI) training, and similar technologies, are reserved.

<https://doi.org/10.1364/OL.557384>

Early disease diagnosis relies on the ability to detect biomarkers at ultralow concentrations, where precise molecular detection plays a critical role in improving clinical outcomes [1]. Optical whispering-gallery-mode (WGM) microcavity sensors have emerged as highly sensitive platforms for such applications, leveraging enhanced light–matter interactions within these miniature resonant structures [2]. WGM microlasers have recently drawn remarkable attention in biosensing due to their high sensitivity and versatile biosensing modalities [3]. It was demonstrated that WGM microlaser sensors can sensitively detect disease biomarkers at an extremely low level [4]. However, the typical method of light coupling with WGM microcavities or microlasers uses a tapered optical fiber with a waist

diameter of smaller than 2 μm , which raises the challenges of on-chip integrated applications due to its high requirements of precise alignment and high susceptibility to environmental disturbances, such as vibrations or contamination. With the use of WGM microlaser sensors, one promising solution is employing the lasing spectra emitted from the sensors for interrogating biosensing signals. However, conventional WGM microlasers typically adopt circular microcavities for achieving high-quality (Q) factors [5,6], resulting in isotropic emission that makes the efficiency of the far-field collection of lasing spectral information low [7].

A promising solution to this issue is to utilize weakly deformed WGM microcavities, which can provide directional emission while maintaining high- Q factors [8,9]. This directional emission property facilitates more efficient coupling of light to waveguides or optical fibers, overcoming the challenges associated with isotropic emission [10]. Despite substantial research into the directionality of deformed microcavities, achieving an optimal balance between emission directionality and Q factor for on-chip biosensing remains a significant challenge, requiring elaborate design and facile fabrication.

In this work, we present a 3D micro-printed WGM microlaser sensor with a limacon-shaped microdisk microcavity. Figure 1(a) depicts the directional emission of a limacon-shaped WGM microlaser sensor overcoming the relatively low far-field collection efficiency in the WGM microlaser sensors with a rotational-symmetric microcavity [4] and the resonance wavelength shift of the WGM microlaser spectrum in response to a change of external refractive index. With a proper choice of deformation coefficient and microdisk radius, both high- Q factor and efficient directional emission can be achieved to overcome the issue of isotropic emission in traditional circular WGM microcavities, which thus provides a promising solution for on-chip integrated biosensing, as shown in Fig. 1(b).

Numerical simulations were conducted to analyze the WGM distributions in a limacon-shaped microcavity made of SU-8 photoresist with a refractive index of 1.57 and reveal its sensitivity to a change of external refractive index. The boundary

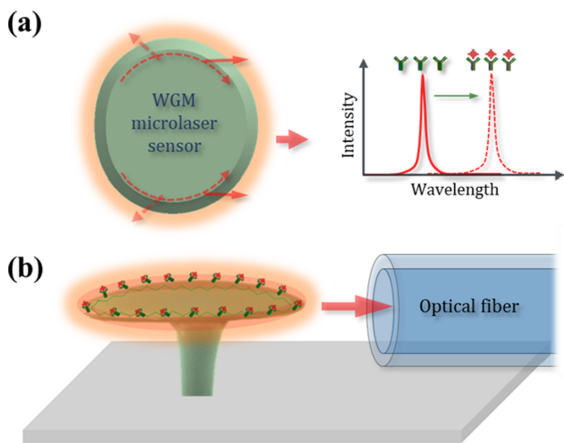


Fig. 1. (a) Schematic of a WGM microlaser biosensor with a limacon-shaped microcavity, showing directional emission and resonance shift in biosensing. (b) Schematic of a 3D micro-printed WGM microlaser sensor in an on-chip sensing platform using optical fiber for light signal collection.

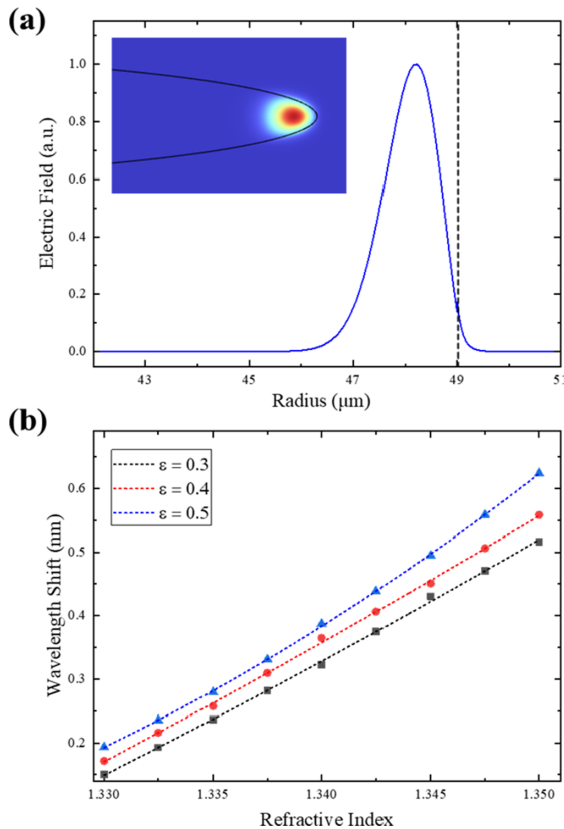


Fig. 2. (a) Simulated electric field distribution of WGMs along the radial direction around the edge of a microcavity. The inset shows the simulated electric field in the cross section. (b) Calculated shift of the peak wavelength of WGMs with respect to a change of external refractive index.

curve of the limacon-shaped microcavity can be described in polar coordinates as $r(\theta) = r_0(1 + \varepsilon \cos\theta)$, where ε is the deformation coefficient for the circle with a radius r_0 . To reduce computational complexity, the refractive index sensitivity of a limacon-shaped WGM microcavity was evaluated by using a

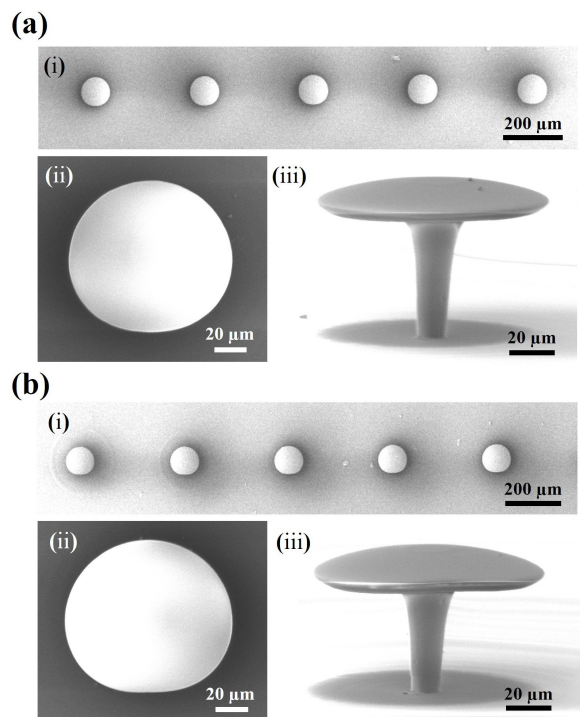


Fig. 3. SEM images of 3D micro-printed SU-8 limacon-shaped WGM microcavities with the deformation coefficient ε of (a) 0.4 and (b) 0.5: (i) array of microcavities, (ii) enlarged top view of a single microcavity, and (iii) enlarged side view (at the view angle of 80°) of a single microcavity.

series of circular SU-8 microcavities. The radii of these circular SU-8 microcavities are obtained from the curvature radius of the limacon-shaped microcavity's contour. The edge of the microcavity is assumed to be an ellipse according to the cross-sectional images of printed samples. Figure 2(a) shows the calculated electric field distribution along the radial direction around the edge of a circular WGM microcavity whose radius R is 49 μm . Its corresponding electric field distribution along the cross section is given in the inset. The calculated wavelength shifts of the WGMs of three limacon-shaped WGM microcavities with different deformation coefficients (i.e., $\varepsilon = 0.3, 0.4, 0.5$) are given in Fig. 2(b). One can see that the peak wavelength of WGMs has a nearly linear response for the refractive index ranging from 1.330 to 1.352. For the WGM microcavities with the deformation coefficients of 0.3, 0.4, and 0.5, the calculated sensitivities are 17.83, 19.28, and 20.92 nm/RIU, respectively, when the external refractive index is around 1.333.

Although high-quality WGMs have been fabricated by many different methods, such as direct femtosecond laser writing [11] and electron-beam (e-beam) lithography [12], they are typically expensive and time-consuming processes. In our earlier works, we have demonstrated an optical 3D micro-printing technique capable of directly printing polymer-based WGM microcavities [13,14]. This method offers high resolution and scalability, enabling the rapid fabrication of complex geometries using different materials. Here, we extend these works to 3D micro-print WGM microlaser sensors with weakly deformed cavities. SU-8 photoresist was used to fabricate WGM microcavities due to its distinct optical property (transparent in both visible and near infrared) and mechanical strength. Octyloxydiphenyliodonium

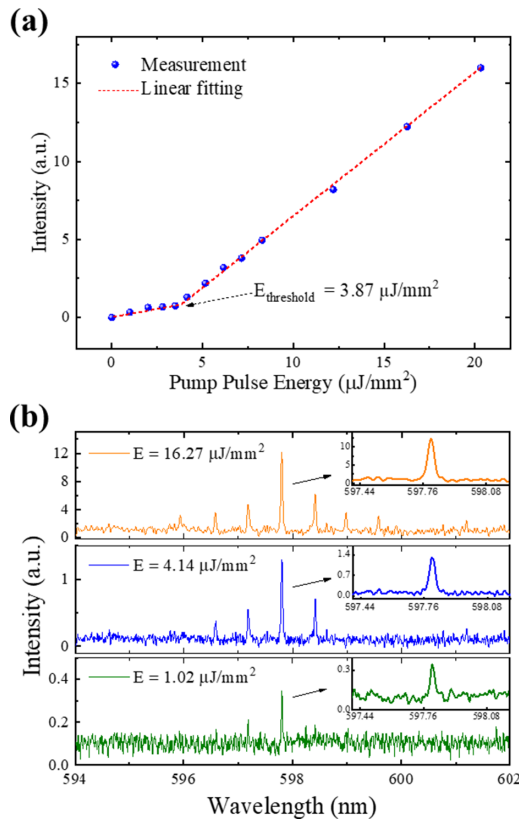


Fig. 4. Measured lasing characteristics of the fabricated WGM microlaser. (a) Measured output intensity as a function of pump pulse energy. (b) Measured emission spectra of the WGM microlaser at pump energies of 1.02, 4.14, and $16.27 \mu\text{J}/\text{mm}^2$.

hexafluoroantimonate (OPPI), TINUVIN 234, and tributylamine (TBA) were added to the photoresist to take the roles as the photo-initiator, UV absorber, and inhibitor, respectively. More details about this printing technology and material preparation can be found in [13–15].

Figure 3 shows the scanning electron microscope (SEM) images of the fabricated SU-8 limacon-shaped WGM microcavities with two different deformation coefficients, i.e., 0.4 and 0.5. The radius of the micro-disks of the WGM microcavities is 49 μm . The height of the microcavities is about 60 μm , designed for on-chip integrated biosensing with standard optical fibers. One can see that the 3D micro-printing technology can quickly fabricate multiple WGM microcavities, and the flat and smooth surface of the fabricated microcavities indicates high- Q factor. To make these WGM microcavities into microlaser sensors, Rhodamine 6 G (Rh6 G) was used to cap microcavities as the optical gain medium because Rh6 G has many advantages such as high quantum yield, high extinction coefficient, excellent photostability, and low toxicity. Rh6 G was mixed with SU-8 photoresist at the concentration of 1.5 wt% and then spin-coated onto the surface of these WGM microcavities.

The lasing characteristics of the WGM microlasers along the $\theta = 0$ direction was tested by using a setup with a nanosecond green laser (MPL-T-532-1; Changchun New Industry Optoelectronics Tech. Co., Ltd.). The central wavelength of the laser is 532 nm, and the laser beam was focused to cover the whole microcavity. Light emitted from the WGM microlasers was collected by using a multimode optical fiber with a core diameter

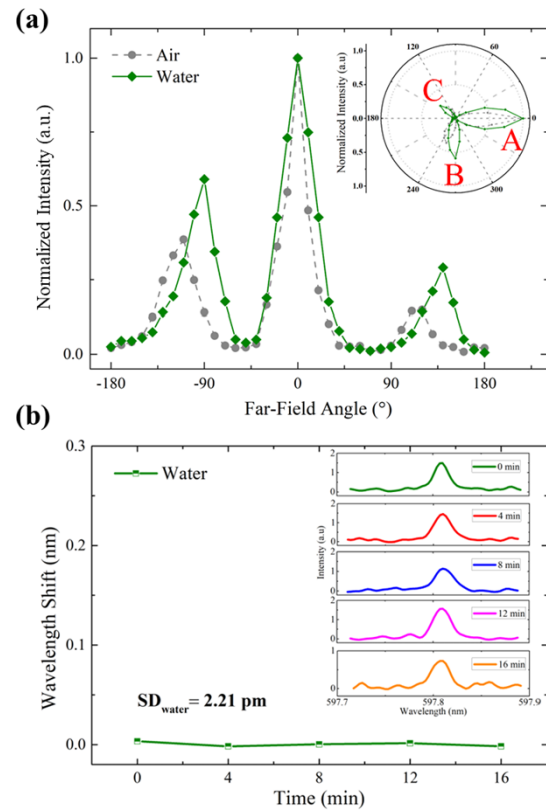


Fig. 5. (a) Measured far-field profiles of a limacon-shaped WGM microlaser over 360° in air and water, respectively. The inset shows the far-field patterns in the polar coordinate system. (b) Stability test result of the WGM microlaser sensor. The inset shows the measured spectra at 4-min intervals.

of 100 μm . The collected light was then analyzed by using a spectrometer (HF-9332; Light Machinery, Ltd.) with a spectral resolution of 25 pm.

The lasing threshold was measured as low as $3.87 \mu\text{J}/\text{mm}^2$, as shown in Fig. 4(a). The measured emission spectra of the WGM microlasers at different pump energies, i.e., 1.02, 4.14, and $16.27 \mu\text{J}/\text{mm}^2$, are presented in Fig. 4(b). As expected, the number of lasing WGMs increased with pump energy. A measured free spectral range (FSR) of 0.67 nm is close to the theoretically estimated FSR, i.e., 0.68 nm. As the suspended microdisk of the WGM microcavity was trimmed to form a micrometer-scale thin edge by a gray-scale exposure technique, only the fundamental transverse mode was excited in the experiments. Using the emission spectrum measured at $4.14 \mu\text{J}/\text{mm}^2$, which is just a bit above lasing threshold, the resonant spectral peak centered at 597.81 nm was fitted using the Lorentzian function, yielding a full width at half maximum (FWHM) of 30.01 pm. Therefore, the Q factor of such an active WGM microcavity under far-field excitation and collection was estimated to be about 2.0×10^4 .

The far-field emission profiles of a limacon-shaped WGM microlaser were measured in both air and water to assess the direction emission property at different surrounding environments. Emission spectra were recorded at pump pulse energies of $10.05 \mu\text{J}/\text{mm}^2$ in air and $16.58 \mu\text{J}/\text{mm}^2$ in water. Distinct emission peaks were observed at 0° , 120° , and 250° in air and 0° , 140° , and 270° in water, as seen in Fig. 5(a). Experimental

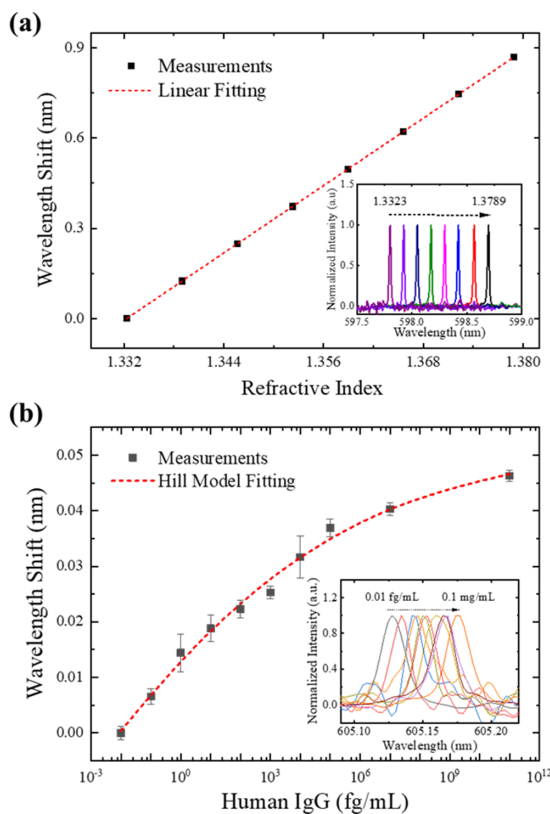


Fig. 6. (a) Measured wavelength shift of the WGM microlaser sensor with respect to the change of external refractive index. Inset shows the measured emission spectra. (b) Testing result of the WGM microlaser biosensor in the detection of human IgG, with data fitted using the Hill model. Inset shows the emission spectra measured in the test.

results verified that the WGM microcavity can achieve directional emission in both air and water environments. The spectral stability of the WGM microlasers was tested in water, as shown in Fig. 5(b). The peak wavelength of the WGM microlaser is very stable, and its standard deviation is 2.21 pm over 16 min.

The bulk sensitivity of the WGM microlaser sensor was tested by using buffer solutions prepared by blending glucose and deionized water. As expected, the peak wavelength of WGMs shifted to longer wavelengths with respect to the increase of external refractive index, as shown in Fig. 6(a). The measured sensitivity was 18.65 nm/RIU, which agrees well with the numerical simulation prediction.

The biosensing performance of the WGM microlaser sensor was tested by using human immunoglobulin G (HIgG), which is a major class of antibody in the blood and extracellular fluids. Its concentration is an important indicator of humoral immune response associated with many types of diseases [16–18]. Before testing, the surface of the WGM microlaser sensor was salinized by using a 4% APTES aqueous solution for 15 min and then rinsed with phosphate-buffered saline (PBS) buffer solution. The sensor was immersed in 100 µg/mL goat anti-human IgG at room temperature for 30 min. After rinsing away unbound antibodies, a 1% bovine serum albumin (BSA) solution was utilized to block nonspecific sites. Finally, a PBS rinse was applied to remove loosely bounded molecules, completing the preparation of WGM microlaser biosensors.

The WGM microlaser biosensor was tested by using HIgG solutions with the concentrations ranging from 0.01 fg/mL to 0.1 mg/mL. Antigen–antibody binding events on the microlaser surface caused redshifts in the WGM resonance wavelength, as shown in Fig. 6(b). Thanks to its wavelength-encoded sensing nature, this WGM microlaser sensor is not sensitive to energy loss caused by the presence of a few small particles or biomolecules. Experimental data fitted with the Hill model reveals a good correlation ($R^2 = 0.97$) between wavelength shift and HIgG concentration. With a noise level of 1.59 pm measured at a concentration level of 0.01 fg/mL, the sensor’s detection limit was estimated to be around 65.5 ag/mL, revealing its great potential for early disease diagnosis. This very low detection limit is primarily due to the resonant nature of the high- Q WGM microlaser sensor and its very narrow linewidth of lasing peaks.

In summary, we have demonstrated an ultra-sensitive polymer WGM microlaser biosensor based on a limacon-shaped microcavity for label-free biodetection. Using a 3D micro-printing technology, the WGM microlaser biosensors have been experimentally fabricated and revealed not only very low lasing threshold but also directional emission property. Moreover, the WGM microlaser sensors can detect antibody HIgG at the concentration level of sub-femtogram per milliliter, which thus may open new opportunities for the development of high-sensitivity lab-on-a-chip devices for diagnostic applications.

Funding. Research Grants Council of the Hong Kong SAR, China (15220721, 15232823).

Acknowledgment. The authors acknowledge the discussions with Prof. Qinghai Song from Harbin Institute of Technology (HIT), Shenzhen.

Disclosures. The authors declare no conflict of interest.

Data availability. Data underlying the results presented in this paper are not publicly available but may be obtained from the authors upon reasonable request.

REFERENCES

- M. S. Pepe, R. Etzioni, Z. Feng, et al., *J. Natl. Cancer Inst.* **93**, 1054 (2001).
- H. Yu, X. Liu, W. Sun, et al., *Opt. Laser Technol.* **177**, 111099 (2024).
- N. Toropov, G. Cabello, M. P. Serrano, et al., *Light Sci. Appl.* **10**, 42 (2021).
- Z. Guo, Y. Qin, P. Chen, et al., *Small* **16**, 2000239 (2020).
- S. Yang, Y. Wang, and H. Sun, *Adv. Opt. Mater.* **3**, 1136 (2015).
- N. Liang, J. Yan, and T. Zhai, *Laser Photonics Rev.* **17**, 2300343 (2023).
- Y. Zhang, Q. Song, D. Zhao, et al., *Opt. Laser Technol.* **159**, 108955 (2023).
- Q. Song, W. Fang, B. Liu, et al., *Phys. Rev. A* **80**, 041807 (2009).
- X.-F. Jiang, C.-L. Zou, L. Wang, et al., *Laser Photonics Rev.* **10**, 40 (2016).
- J. Wiersig and M. Hentschel, *Phys. Rev. Lett.* **100**, 033901 (2008).
- Y.-L. Sun, Z.-S. Hou, S.-M. Sun, et al., *Sci. Rep.* **5**, 12852 (2015).
- S. F. Wondimu, M. Hippler, C. Hussal, et al., *Opt. Express* **26**, 3161 (2018).
- J. Wu, X. Guo, A. P. Zhang, et al., *Opt. Express* **23**, 29708 (2015).
- X. Ouyang, T. Liu, Y. Zhang, et al., *Lab Chip* **20**, 2438 (2020).
- Z. Wang, Y. Qin, and A. P. Zhang, *CLEO, Technical Digest Series* (Optica Publishing Group, 2023), paper Atu3R.2.
- N. Niu, J. Zhang, Y. Guo, et al., *Int. J. Biochem. Cell Biol.* **43**, 556 (2011).
- S. Huseynli, G. Baydemir, E. Sari, et al., *Mater. Sci. Eng.: C* **46**, 77 (2015).
- E. Melnik, R. Bruck, P. Müllner, et al., *J. Biophotonics* **9**, 218 (2016).